ISSN 1590-8844
International Journal of Mechanics and Control, Vol. 17, No. 01, 2016

MAGNETIC AND STRUCTURAL CO-DESIGN OF SYNCHRONOUS RELUCTANCE ELECTRIC MACHINES IN AN OPEN-SOURCE FRAMEWORK

Simone Ferrari Gianmario Pellegrino Elvio Bonisoli

Politecnico di Torino, corso Duca degli Abruzzi, 24 – 10129 Torino Italy

ABSTRACT

Synchronous reluctance motors (SyRM) produce torque thanks to the rotor magnetic anisotropy, without use of permanent magnets (PMs) or windings on their rotor. Consequently, SyRMs are cost-competitive against costly PM synchronous machines and more efficient than asynchronous motors, because of the absence of the squirrel cage and related Joule loss in the rotor. The SyR motor's rotor laminations have air cavities called flux barriers carved in each pole to maximize anisotropy and torque. The rotor iron parts, called flux carriers, are kept together by tiny pieces of steel called the structural ribs, which withstand significant centrifugal stress at high operating speed. If the ribs size is increased, more flux bypasses the flux barriers are bypassed and the reluctance torque diminishes. Altogether, magnetic anisotropy and structural integrity need a proper co-design strategy to be formulated. Since magnetic design relies on non-negotiable 2D finite element model (FEM) analysis, using 2D-FEM also for centrifugal stress evaluation would lead the computational burden to unacceptable levels. The paper develops a comprehensive co-design methodology based 2D magnetic FEM and beam structural analysis (1D-FEM), that limits the size of the structural problem and make extra time dedicated to structural computation negligible.

Keywords: synchronous reluctance machine, design of electrical machines, magnetic and structural co-design, high speed rotors, high speed electrical machines

1 INTRODUCTION

Synchronous Reluctance machines (SyRMs) are a class of AC electrical machines renowned for their high-efficiency and convenient manufacturing cost [1-3]. They are more efficient than asynchronous machines and less expensive than permanent magnet synchronous machines, because of the absence of magnets. Recently, they have been considered for high-speed applications [4-5]. The stator of a SyRM resembles the one of a standard induction motor (IM). Design wise, the most important part of a SyRM is the rotor. Synchronous reluctance torque (1) is maximised by maximization of the difference between the *d*- and *q*-axis inductances:

$$T = \frac{3}{2} p \cdot (L_d - L_q) \cdot I_s \cdot \frac{\sin(2\gamma)}{2} - \Delta T_{ribs} \quad (1)$$

where *d* and *q* are the rotor directions defined in Fig. 1, I_s is the amplitude of the stator phase current and γ is the phase angle of the current vector in the *dq* reference frame, synchronous to the rotor. The two inductances L_d and L_q summarize the properties of the two rotor axes: *d* is the direction of maximum permeability (Fig. 1a), whereas *q* is the direction of maximum reluctance (Fig. 1b).

The reluctance comes from the presence of the rotor cavities, called the flux barriers. The difference (L_d - L_q) determines the reluctance torque of the machine (1). A subtractive torque component comes from the rotor ribs flux linkage λ_{ribs} [Vs], that is the flux that bypasses the flux barriers in the *q* direction via the structural ribs. Such ribs, defined in Fig. 2, keep together the rotor parts. Their negative impact on torque is roughly proportional to the sum of their widths (w_{rib}):

$$\Delta T_{ribs} = \lambda_{ribs} \cdot I_s \cdot \cos(\gamma) \propto \sum_{j=1}^{nribs} w_{rib,j} \quad (2)$$

Contact author: Simone Ferrari

Email: simone.ferrari@polito.it

The design of high-speed SyRM rotors requires that (2) is minimized while structural integrity at maximum speed is retained. The key point of such tradeoff is the design of the structural ribs.

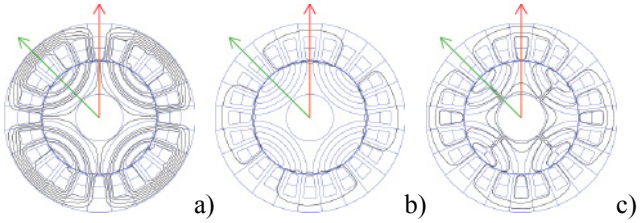

Figure 1 Flux lines when the two main rotor directions (d = red, q = green) are magnetized with the same peak current. a) d-axis; b) q-axis, with tangential ribs; c) q-axis, with tangential and radial ribs.

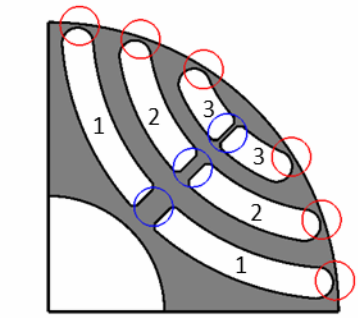

Figure 2 Red: tangential ribs. Blue: radial ribs.

Fig. 2 illustrates the two types of structural ribs investigated in this paper: tangential (red) and radial (blue). Tangential ribs cannot be omitted and their minimum size is normally dictated by the thickness of the lamination and the cutting process. For low speed applications they can guarantee the structural integrity of the rotor without additional radial ribs. Conversely, in high-speed applications the centrifugal force becomes too high and radial ribs (blue) are included. The insertion of the radial ribs further reduces the reluctance torque of the SyR machine, according to (1) and (2).

The design tool adopted in this paper is SyR-e [6], an open-source design platform written in Matlab and based on the 2D magnetic simulation engine FEMM [7]. SyR-e uses multi-objective differential evolution (MODE) and FEMM to optimize the shape and size of the SyRM rotor barriers. A simple ribs stress formulation is adopted, to design the radial ribs thickness according to speed. The tangential ribs are set to a constant thickness, according to the cutting process, as said. The design approach of SyR-e becomes more and more imprecise at higher rotational speeds. A better way to include structural co-design of the ribs into SyR-e would be to use a 2D-FEM (shell) also for the structural design. In this case, the integration between magnetic and structural FEM would not be trivial and computing time could become very long.

This paper studies the feasibility of using 1D-FEM analysis for the structural design part, based on beam elements [8, 9]. The 1D-FEM requires a limited computing time, so that the total computational time of one machine design in SyR-e remains nearly the same. Moreover, the 1D-FEM mesh creation is much easier to integrate into the magnetic design pipeline.

The paper is organized as follows. First, the automatic construction of the 1D mesh of the SyRM rotor is addressed. Then, the accuracy of the 1D-FEM model is assessed against linear and nonlinear 2D-FEM. Finally, a magnetic and structural co-design strategy is defined and implemented in SyR-e.

2 1D-FEM MODEL

The 1D-FEM model, objective of this work, will be validated against the results of the more accurate and time consuming 2D structural FEM, using triangular mesh elements of the second order in SolidWorks (CTRIA6).

2.1 LINEAR VS NON-LINEAR 2D MODEL

Linear and nonlinear 2D-FEM results are compared in this section. Two simulations of the same rotor are carried out, with the same mesh (6217 nodes, 2689 elements, curvature based mesh), and the same rotational speed (50000 rpm, tip speed 157 m/s), one in the linear case and the other one considering the non-linear strain-stress curve of the M530-65A electrical steel. The computing time was about 10 seconds for the linear case and 15 minutes for the nonlinear one.

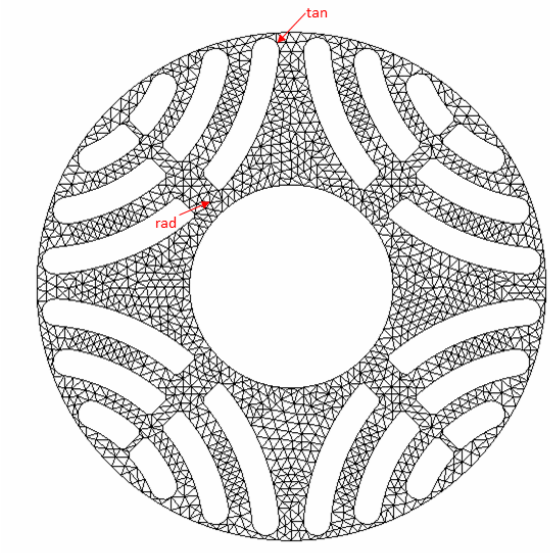

Figure 3 Mesh of the 2D-FEM used for the comparison between linear and non-linear model (6217 nodes, 2689 elements, curvature based mesh).

The Von Mises equivalent stress in the most loaded tangential e radial ribs are reported in Fig. 4. In both cases the tangential ribs exceeds the yield strength, but the

nonlinear model tells that the ultimate tensile strength is not exceeded. Indeed, the linear model overestimates stress by far, in case the yield limit is trespassed. Dealing with the radial ribs results, stress is far from the yield limit according to both models. The conclusion is that if the radial rib is strong enough, then the rotor can survive from the plasticisation of the tangential ribs [10]. Plus, under this assumption, the stress in the radial rib is modelled fairly well also by the linear model. Therefore, for simplicity, the 1D-FEM model will use a linear steel model and non-linear simulation will be used for validation with 2D-FEM.

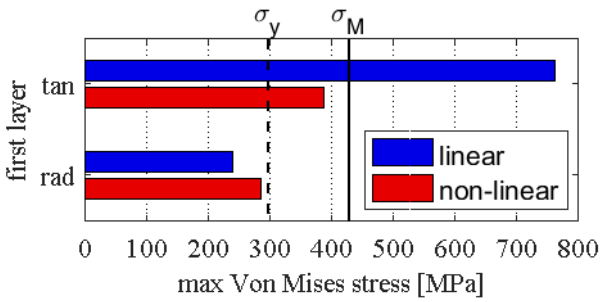

Figure 4 Results from 2D linear and non-linear simulations.

2.2 AUTOMATIC BEAM CONSTRUCTION

One pole of rotor lamination is modelled with a beam structure. An automatic procedure is implemented for integrating the beam model construction into SyR-e. First of all, a set of nodes is automatically placed in key positions of the structure, as represented in Fig. 5a. After the nodes, the beams are defined, as show in Figure 5b. The ribs are modelled as single beams. The width of the beam connected to the tangential ribs is calculated from the radius of the end-arc of the flux barrier and the width of the tangential rib. The width of the terminal beam of the inner flux carrier is calculated from the distance between the ends of the end-arc of the nearby flux barriers.

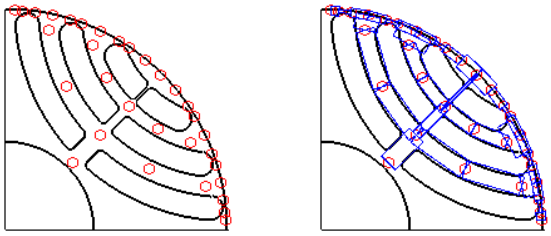

a) b)

Figure 5 a) nodes and b) beam of the 1D-FEM.

2.3 CENTRIFUGAL FORCES

One radial force is associated to each beam, applied to its centre of mass, taking into account the centrifugal load:

$$F = A \cdot h \cdot \rho \cdot r \cdot \omega^2 \quad (3)$$

where A [m^2] is the cross section of the rectangular beam, h [m] the axial thickness, ρ [kg/m^3] the material density, r [m] the distance between the centre of mass and the rotation axis and ω [rad/s] is the rotational speed.

Figure 6 shows the areas presenting some exceptionality in the construction process of beam and forces. The green area around tangential ribs consists of three beams, with only one force associated, applied to the node in common to the three beams. The area highlighted in yellow in Figure 6 is considered in place of the entire beam area, for the radial ribs. Finally, the beams in the external flux carrier use the polygonal areas highlighted in cyan and magenta.

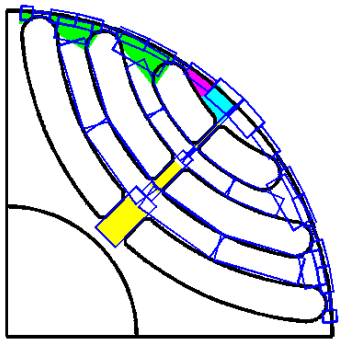

Figure 6 Beam structure and areas with exceptions in the evaluation of centrifugal forces.

2.4 VALIDATION

The 1D-FEM approach is validated using linear 2D-FEM, as said. The reference rotor geometry is shown in Figure 7 and summarized in Table I. At first, only the tangential ribs are considered, at 15000 rpm. Later, simulations at higher speed levels are carried out, with insertion of radial ribs of progressive size. The layers are numbered from the innermost to the outermost as indicated in Figure 2. The equivalent Von Mises stress of the beams representing the ribs is considered.

Table I - Dimensions of the design example.

Rotor diameter	mm	30
Maximum speed	rpm	15000
Tangential ribs thickness (nominal)	mm	0.4

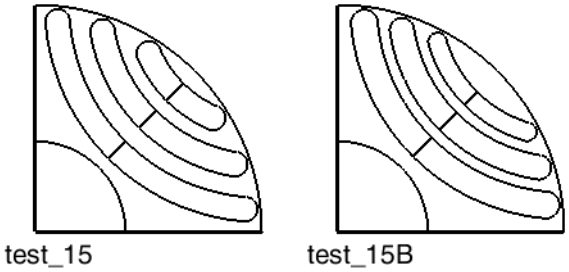

Figure 7 Test geometry for the comparison between 1D-FEM and 2D-FEM.

2.2.1 Test with nominal tangential ribs

The simulations are performed at 15000 rpm. The dimension of the tangential ribs is the nominal one, equal to 0.4 mm. This corresponds to the lower limit of the manufacturing process. The computing time of the 1D-FEM is lower than 1 second.

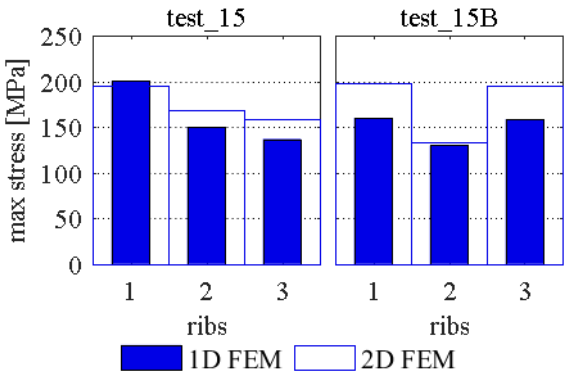

Figure 8 Maximum Von Mises stress of the laminations without radial ribs evaluated with 1D-FEM and 2D-FEM.

2.2.2 Tests with radial ribs

These laminations are obtained starting from the same basic geometry of test_15 (fig. 7a) and setting a higher levels of maximum speed in SyR-e. SyR-e can design the radial ribs according to speed, using a simplified structural model, as said. The three cases are summarised in Table II. At 25000 rpm the machine has one radial rib in layer one, at 30000 rpm two radial ribs (layers 1 and 2), and at 50000 rpm three ribs. The ribs thicknesses are reported in Table II. The dimension of the tangential ribs is 0.4 mm for all the rotors. Figure 9 reports the maximum Von Mises stresses of the laminations with radial ribs evaluated with 1D and 2D-FEM. Overall, the proposed 1D-FEM approach represents the centrifugal stress quite accurately. Errors are in the range of 20%, considering the most significant point of each lamination.

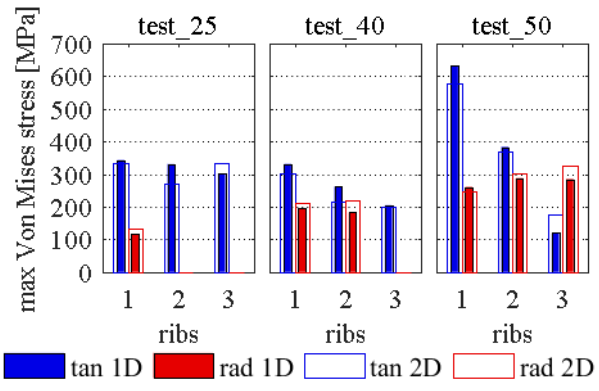

Figure 9 Maximum Von Mises stress of the laminations with radial ribs evaluated with 1D-FEM and 2D-FEM.

Table II - Dimension of the radial ribs.

Name	Speed (rpm)	Radial rib 1 (mm)	Radial rib 2 (mm)	Radial rib 3 (mm)
test_25	25000	0.7	/	/
test_30	30000	1.0	0.5	/
test_50	50000	2.6	1.3	0.4

3 MAGNETIC AND STRUCTURAL CO-DESIGN

This section analyses the magnetic and structural effect of ribs widths, to help defining a correct method to design the tangential and radial ribs. Two sets of rotor lamination are considered, derived from the geometry of test_15 (see Fig. 7a). A first set of laminations have all tangential ribs progressively increased by 0.2 mm, 0.5 mm, 1 mm and 1.5 mm, respectively, leading to a total ribs width increase of 0.4 mm, 1.0 mm, 2.0 mm and 3.0 mm per each layer. In the second set of rotors, the tangential ribs are all at 0.4 mm, as in the baseline geometry, and radial ribs are progressively inserted, using the same reference quantities (0.4, 1.0, 2.0, 3.0 mm). Table III reports the dimensions of the ribs for of the rotor laminations used for these tests.

Table III – Designs with augmented ribs dimensions.

Name	Width of tang. ribs (mm)	Width of rad. ribs (mm)	Total increase (mm)
base	0.4	/	/
R04	0.4	0.4	0.4
T04	0.6	/	0.4
R10	0.4	1.0	1.0
T10	0.9	/	1.0
R20	0.4	2.0	2.0
T20	1.4	/	2.0
R30	0.4	3.0	3.0
T30	1.9	/	3.0

3.1 EFFECT OF RIBS SIZE ON TORQUE AND SPEED LIMITS

Torque is computed with 2D magnetic FEM through SyR-e for all the considered rotors. All simulations refer to the same current loading conditions (90 A/mm), in amplitude and phase. According to (2), with the same current, torque will decrease in inverse proportion of the ribs size. Figure 10 shows the output torque as a function the total ribs increase in [mm]. The bars at 0 mm represent the baseline rotor (test_15 of Fig. 7), which is intuitively the one giving the highest torque. For the same width increase (e.g. 3 mm), radial ribs have a stronger impact on torque.

2D-FEM linear analysis is used to compare the same set of rotors in terms of maximum stress at constant speed (Fig. 11a). Consequently, the maximum speed capability of each machine is evaluated, imposing that the ribs stress equals the yield limit (Fig. 11b). Given the results of the simulation at n_0 = 15.000 rpm, speed can be increased as far

as the yield point is touched. In the linear case, stress is proportional to the square of the speed, leading to:

$$n_{\max} = n_0 \cdot \sqrt{\frac{\sigma_{yield}}{\sigma_0}} \tag{4}$$

where n_{max} [rpm] is the mechanical speed limit, n_0 = 15000 rpm is the test speed, σ_{yield} [MPa] is the yield strength of the steel and σ_0 [MPa] is the stress evaluated in the test simulations. The two figures put in evidence that radial ribs have a way stronger impact on structural strength than tangential ribs, although they penalize torque production slightly more.

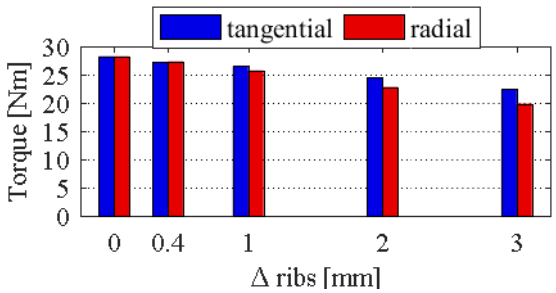

Figure 10 Torque versus increase on ribs, at given current conditions.

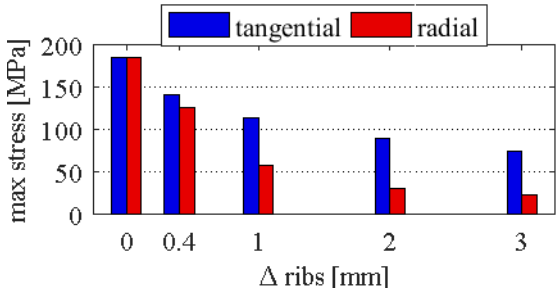

a)

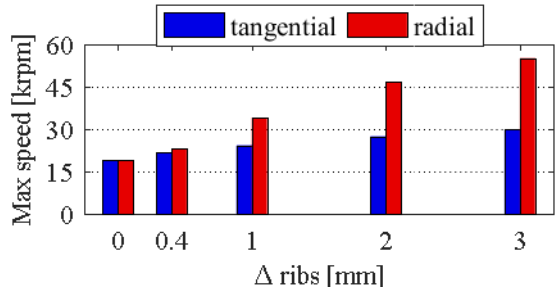

b)

Figure 11 a) Max Von Mises stress versus ribs growth at 15000 rpm. b) Maximum speed limit of the geometries with augmented ribs.

3.3 CO-DESIGN STRATEGY

The co-design strategy must be developed from the magnetic and structural analysis. The maximum torque and speed is not the real maximum characteristics of the machine, because they depend also from the power supply. The values obtained from these analyses are the upper limits, due to the rotor geometry. To join the two analysis, all the test machines are plotted in the torque-speed plane (Figure 12). Near the dots who represent the machine, it is shown the name of the machine (see Table III for the dimension of the ribs). The chart shows that the best solution to improve the mechanical characteristic of the rotor lamination is using the radial ribs, indeed they allow to provide a higher torque than increasing the tangential ribs, at the same speed. Moreover, they allow reaching higher power than increasing only the tangential ribs. The only disadvantage of the radial ribs is the minimum dimension (0.4 mm for this example): The red characteristic from base to T04 does not exist because of the small width of the radial ribs. The co-design algorithm will follow the green line: before the tangential ribs will be increased, until 50% plus than the base width; than the radial rib will be inserted and the tangential ribs will revert to the base width. This method will be applied for each layer.

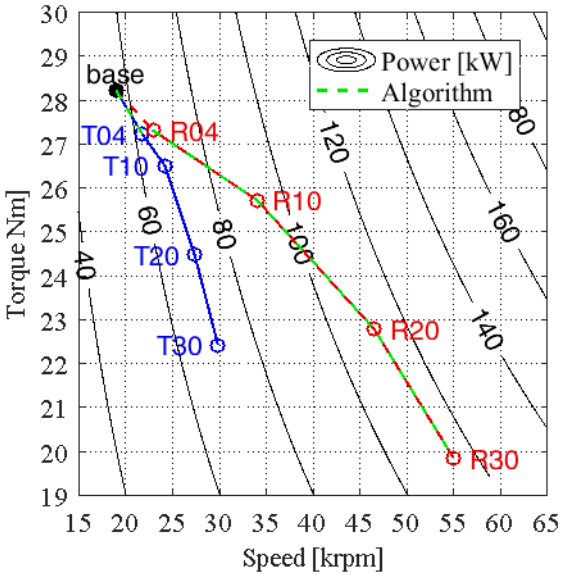

Figure 12 Magnetic and structural analysis on the torque-speed plane.

The algorithm is based on a loop. Before the loop, some block build the 1D-FEM automatically and do a preliminary design of the ribs. This preliminary design check the stress in the tangential ribs and, if the maximum stress is higher than the yield strength, the procedure calculate the new width of the tangential ribs which allows to have the maximum stress equal to the yield strength. The evaluation formula is the (5), where w [mm] is the width of the ribs, σ [MPa] is the stress, with *old* is shown the previous value and with *new* is showed the new value. This formula is not exact, but it gives an easy way to change the dimension of the ribs, using the stress. The loop will correct the errors.

$$w_{new} = w_{old} \cdot \frac{\sigma_{old}}{\sigma_{\max}} \tag{5}$$

If the new width of the tangential ribs is higher than 1.5 times the minimum width of the ribs, then the radial rib will be added, with a dimension calculated from the (6). In this formula w [m] is the width of the radial rib, M [kg] the mass supported from the rib, r [m] is the distance between the centre of mass and the rotation axis, σ_{max} [Pa] is the yield strength and h [m] is the axial width of the rib. This equation ignore the structural effect of the tangential ribs, but all the errors will be correct after some iteration of the loop.

$$w = \frac{M \cdot r \cdot \omega^2}{\sigma_{\max} \cdot h} \tag{6}$$

In the loop, first of all the 1D-FEM is simulated, and then all the layers are checked. If exist the radial rib, the stress of the tangential ribs is ignored. For each layer, the algorithm check if the significant stress is into a defined range (the range used for the evaluation is 95%÷100% of yield strength). If the stress is out of the bounds of the range, the (5) is used to correct the width of the ribs. The width of the tangential ribs is limited in the range 1÷1.5 of the minimum width. If at the maximum width, the stress of the tangential ribs is over the yield strength, then the radial rib is added. The width of the radial ribs is only bounded below at the minimum width of the ribs. The principle of the algorithm is sketch in a simpler and compact form in Figure 13.

4 COMPARISON BETWEEN OLD AND NEW CO-DESIGN PROCEDURES

Starting from the rotor geometry test_15 (Figure 7) it is designed two sets of rotor lamination, the first set is designed with the old algorithm of SyR-e, and the second is designed using the method proposed in this paper. The input of the design is the maximum speed of the motor, and no safe coefficient is applied in the mechanical design: the stress target for the radial ribs is the yield strength.

4.1 RIBS WIDTH VERSUS SPEED

The Figure 14 shows the dimension of the ribs versus the design speed. The machines designed with the proposed method are shown in green, while the machines designed with the actual method (SyR-e) are shown in blue. The old method acts only over the radial ribs, keeping constant the tangential ribs width, while the new algorithm changes also the tangential ribs. The new algorithm insert the radial ribs at lower speed than the old method, this fact points out a lack in the old method. Plus, the new method allows to insert a smaller rib for the first layer, for mid-high speed. You can also see that the layers depend on each other, indeed the insertion of the third radial rib (39000 rpm), causes an increase of the width of the others radial ribs.

4.2 TORQUE VERSUS SPEED COMPARISON

Another relevant comparison between the old method and the new algorithm can be performed in the torque-speed plane, as show in Figure 15. The blue plot show the motor designed with the old method of design and the green plot show the motor designed with the new method. You can see that the new method allows to design, for a mid-high speed (from 20000 to 60000 rpm), more performing machine, with an higher torque (and then an higher power). This is caused from the smaller width of the first radial rib of the machines designed with the new method. At high speed (over 60000 rpm) the new method design worst machine than the old way to design, but performing a first fast structural test (with the 1D-FEM), it turns out that most of the machine designed with the old method (15 of 24) have some mechanical problem, while the machines designed with the new algorithm haven't structural problem.

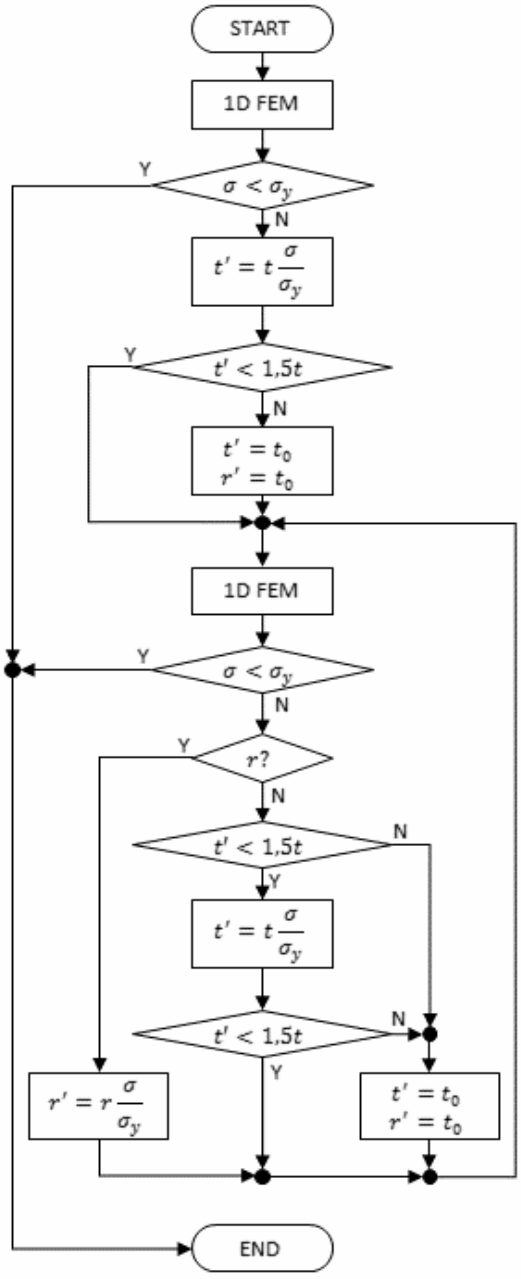

Figure 13 Principle of the proposed co-design algorithm.

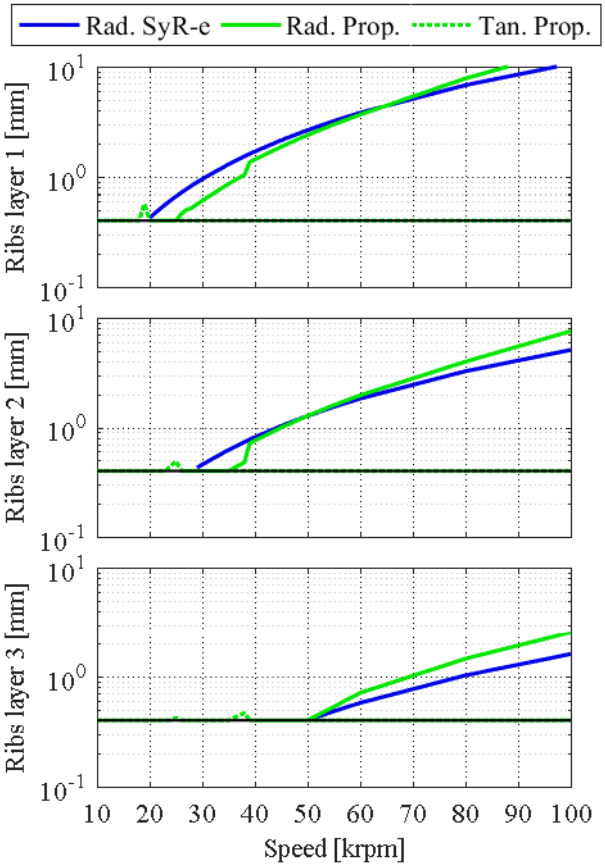

Figure 14 Ribs width comparison for each layer between the machine designed with the proposed algorithm (green) and the machine designed with the old SyR-e (blue).

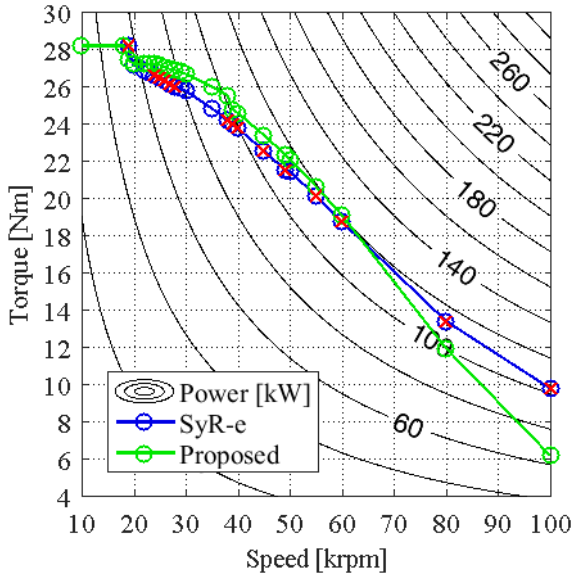

Figure 15 Comparison between the old method and the new algorithm of design on the torque-speed plane.

4.3 STRESS VERIFICATION WITH NON-LINEAR 2D-FEM

In order to check the correct structural design, all the designed machines are simulated with 2D-FEM and a non-linear model of the material. The results are sum up in Figure 17, Figure 18 and Figure 19. You can note that in the first layer (Figure 17), the old algorithm designs oversized machines (the stress in the radial ribs is much lower than the yield strength), but the new algorithm make some errors because some machines have the maximum stress equal or little higher than the yield strength. In the other layers, the behaviour is the same, with less range of speed where the new algorithm make mistakes. Anyway, the stress never reach the ultimate tensile strength, so, all the motor do not break because of the maximum speed. Some problem can be caused from fatigue, but it is not the intent of this paper.

In Figure 16 all the machines designed are shown. The orange crosses mark the machines that have the maximum stress over the yield strength and under the break strength. No one machine reach the ultimate tensile strength, but the very high-speed machines (over 80000 rpm) have a maximum stress closer to the ultimate tensile strength. For the new method 18/24 machines reach the yield strength, while for the old method, only 16/24 machines reach this limit. This is easily avoidable using a safe coefficient in the design method.

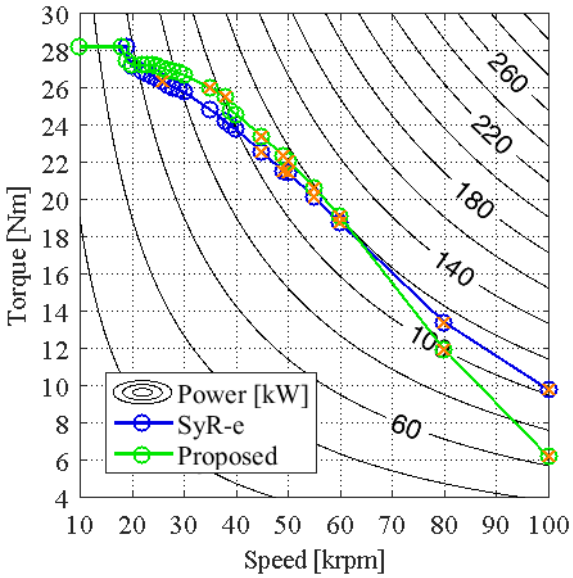

Figure 16 Comparison between the old method and the new algorithm of design on the torque-speed plane and tested with 2D-FEM.

5 CONCLUSIONS

This paper presents a new method of design for SyR machines. The innovations introduced are: the definition of a generalized method to create a 1D-FEM of the SyR

machine's rotor; and the chance to use the 1D-FEM in the design pipeline of SyR motors. It is also investigates the magnetic and structural differences between tangential ribs and radial ribs, and the importance in the choice of the material model for the structural analysis.
Finally, the new method of design, using the 1D-FEM is applied and compared to the old method, showing the advantages in the design, avoiding the high oversizing applied by the old method. The disadvantage is the approximation of the 1D-FEM, which can cause an undersize of the radial ribs and then too high stresses, which can exceed the set limit.

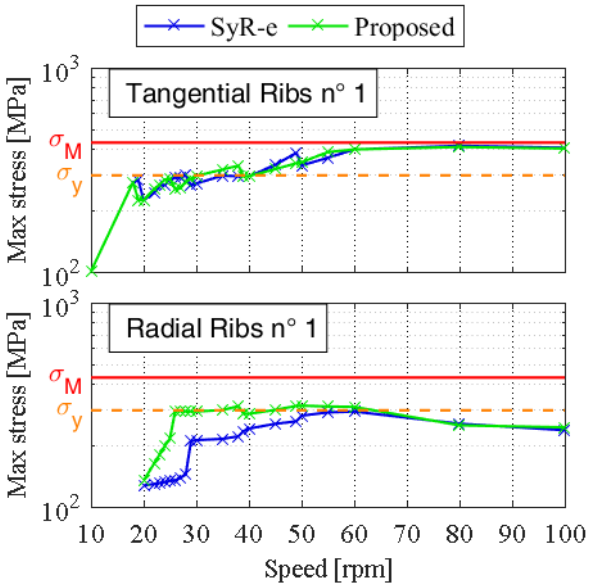

Figure 17 Stress in the first layer evaluated with 2D non-linear FEM.

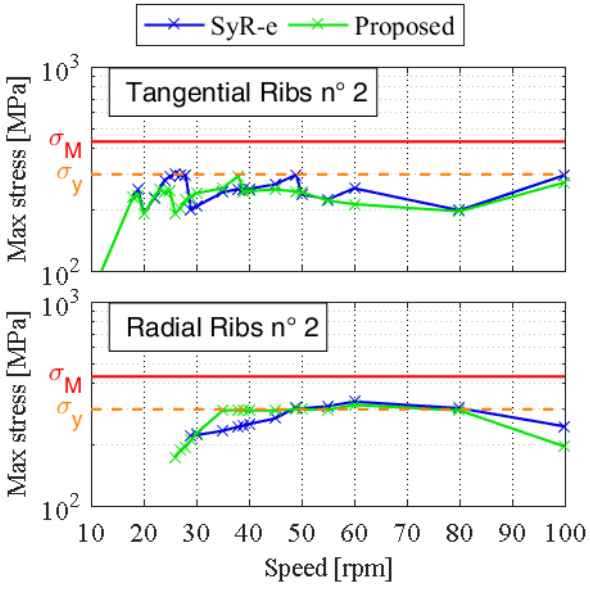

Figure 18 Stress in the second layer evaluated with 2D non-linear FEM.

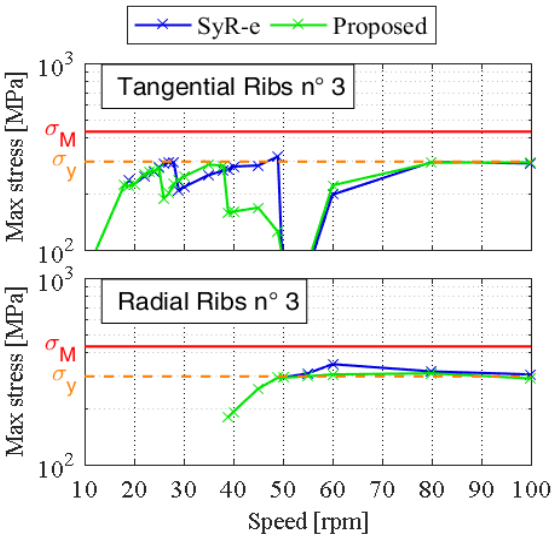

Figure 19 Stress in the third layer evaluated with 2D non-linear FEM.

REFERENCES

[1] *Rotating Electrical Machines—Part 30-1: Efficiency classes of line operated AC motors*. (IE-Code), Ed. 1, IEC 60034-30-1, Dec. 2014.

[2] Vagati A., Fratta A., Franceschini G., Rosso P., AC motors for high-performance drives: a design-based comparison. *IEEE Transactions on Industry Applications*, Vol. 32, No. 5, pp. 1211-1219, Sep/Oct 1996.

[3] Moghaddam R.R., Magnussen F., Sadarangani C., Theoretical and experimental re-evaluation of synchronous reluctance machine. *IEEE Transactions on Industrial Electronics*, Vol. 57, No. 1, pp. 6-13, Jan. 2010.

[4] Di Nardo M., Galea M., Gerada C., Palmieri M., Cupertino F., Multi-physics optimization strategies for high speed synchronous reluctance machines. *2015 IEEE Energy Conversion Congress and Exposition (ECCE)*, Montreal, QC, pp. 2813-2820, 2015.

[5] Ikäheimo J., Kolehmainen J., Känsäkangas T., Kivelä V., Moghaddam R.R., Synchronous high-speed reluctance machine with novel rotor construction. *IEEE Transactions on Industrial Electronics*, Vol. 61, No. 6, pp. 2969-2975, June 2014.

[6] Pellegrino G., Cupertino F., *SyR-e User's Manual ver 1.0*. available online at www.sourceforge.net.

[7] Meeker D., *FEMM Reference Manual*. available online at www.femm.info/wiki/HomePage.

[8] Bathe K.J., F*inite element procedures*. Prentice-Hall, New Jersey, 1996.

[9] Hughes T.J.R., *The finite element method*. Prentice-Hall, New Jersey, 1987.

[10] Juvinall R.C., Marshek K.M., *Fundamentals of machine design*. 5th Ed., Wiley & Sons, 2011.